ADVANCED FUNCTIONAL MATERIALS
www.afm-journal.de

www.MaterialsViews.com

Stepwise Drug-Release Behavior of Onion-Like Vesicles Generated from Emulsification-Induced Assembly of Semicrystalline Polymer Amphiphiles

*Mi-Kyoung Park, Sangmi Jun, Inhye Kim, Seon-Mi Jin, Jin-Gyu Kim, Tae Joo Shin, and Eunji Lee**

Tailoring unique nanostructures of biocompatible and degradable polymers and the consequent elucidation of shape effects in drug delivery open tremendous opportunities not only to broaden their biomedical applications but also to identify new directions for the design of nanomedicine. Cellular organelles provide the basic structural and functional motif for the development of novel artificial nanoplatforms. Herein, aqueous onion-like vesicles structurally mimicking multicompartmentalized cellular organelles by exhibiting exquisite control over the molecular assembly of poly(ethylene oxide)-*block*-poly(ε-caprolactone) (PEO-*b*-PCL) semicrystalline amphiphiles are reported. Compared to in situ self-assembly, emulsification-induced assembly endows the resulting nanoaggregates of PEO-*b*-PCL with structural diversity such as helical ribbons and onion-like vesicles through the molecular packing modification in the hydrophobic core with a reduction of inherent crystalline character of PCL. In particular, onion-like vesicles composed of alternating walls and water channels are interpreted by nanometer-scale 3D visualization via cryogenic-electron tomography (cryo-ET). Interestingly, the nature of the multi-walled vesicles results in high drug-loading capacity and stepwise drug release through hydrolytic cleavage of the PCL block. The crystalline arrangement of PCL at the molecular scale and the spatial organization of assembled structure at the nanoscale significantly affect the drug-release behavior of PEO-*b*-PCL nanovehicles.

1. Introduction

Among the polymer scaffolds, amphiphilic block copolymer, consisting of hydrophobic and hydrophilic blocks, enables not only the facile fabrication of various core–shell nanoarchitectures such as spheres, cylinders, ribbons, and vesicles through aqueous self-assembly[1–3] but also the development of novel functional nanomaterials by incorporation of a specific building block with desired functions.[4,5] Indeed, aqueous nanoparticles of biocompatible and degradable poly(ethylene oxide)-*block*-poly(ε-caprolactone) (PEO-*b*-PCL) diblock copolymer have been formulated to broaden their applications in many biomedical areas.[6–8] In particular, the hollow polymersome has been thoroughly studied due to its confined hydrophilic core and hydrophobic wall spaces, allowing the loading of chemical payloads, including therapeutic and diagnostic agents.[9–11] Recent advances in state-of-the-art self-assembly nanotechnology offer the opportunity to biomimic the complex multicompartmentalized structures in cellular organelles, including multivesicular and multilamellar structures of endosome,[12] multilamellar bodies,[13] myelin,[14] and endoplasmic reticulum,[15] from the structural, mechanical, and functional perspectives.[16,17] However, the simple vesicular structure of PEO-*b*-PCL formed by the direct aqueous self-assembly (referred to as the in situ self-assembly hereafter) has rarely been reported due to difficulties in controlling the degree of PCL semicrystallinity to form fibrils and 2D sheets.[18] In this respect, devising a facile fabrication of complex vesicular nanostructures of PEO-*b*-PCL is still an intriguing subject.

Meanwhile, the shape effects of polymer nanoparticles used in drug delivery have been recognized as an important issue in the development of efficient and effective carriers.[6–8] Both experimental[19] and theoretical studies[20,21] have been conducted. Discher's group reported that PEO-*b*-PCL filomicelles remain in the circulation up to ten times longer in vivo than do spherical micelles and effectively deliver the anticancer drug.[19] Theoretical prediction using molecular dynamics simulation by Vácha et al. demonstrated that the cellular uptake capacity of filomicelles is enhanced compared to that of spherical micelles, and the edge sharpness of filomicelle further affects their internalization.[20,21] Based on these results, one can envision that

M.-K. Park, I. Kim, S.-M. Jin, Prof. E. Lee
Graduate School of Analytical Science and Technology
Chungnam National University
99 Daehak-ro, Yuseong-gu,
Daejeon 305-764, Republic of Korea
E-mail: eunjilee@cnu.ac.kr
Dr. S. Jun, Dr. J.-G. Kim, Prof. E. Lee
Division of Electron Microscopic Research
Korea Basic Science Institute (KBSI)
169-148 Gwahak-ro, Yuseong-gu,
Daejeon 305-806, Republic of Korea
Dr. T. J. Shin
UNIST Central Research Facilities
& School of Natural Science
UNIST, Ulsan 689-798, Republic of Korea

DOI: 10.1002/adfm.201501595

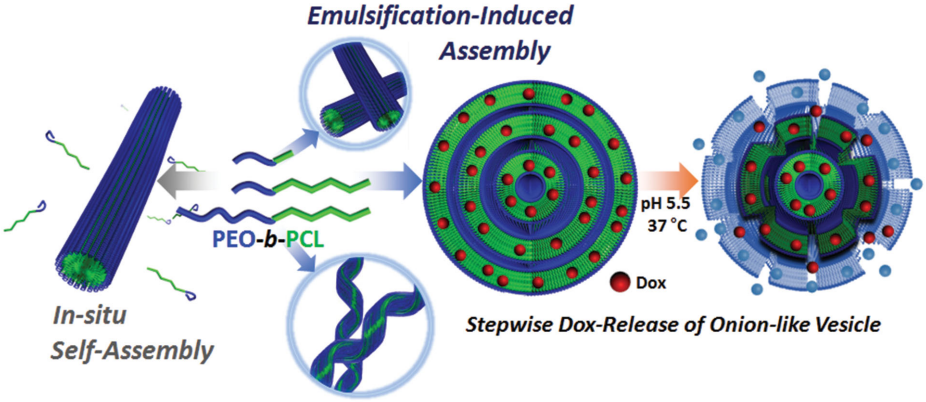

Figure 1. Schematic representation showing the generation and control of nanostructures of PEO-*b*-PCL. Two distinct methods, in situ self-assembly and emulsification-induced assembly, were utilized. Onion-like vesicles formed by the solvent-evaporation of o/w emulsion droplets presented the unique stepwise drug-releasing behavior.

the unique nanostructures of biofunctional polymer, such as complex vesicular nanostructures, would offer new opportunities for the use of nanomedicine in disease treatment and diagnosis.

The precise control of nanostructures formed from the self-assembly of amphiphilic block copolymer was attempted using synthetic modification of polymer parameters (e.g., the relative weight ratios of each block, total molecular weight, and conformation).[22] However, Zhu and Hayward recently reported that the induction of chemical instability of block copolymer at the emulsion droplet interface, during the evaporation of solvent, could be the versatile assembly driving force to obtain exquisite micro- and nanostructures,[23–25] compensating for cost-ineffectiveness and time-consuming chemical synthesis.[26] To this end, we speculated that PEO-*b*-PCL emulsification/solvent-evaporation would generate structural diversity in nanoparticulation and allow us to understand the relationship between such nanovehicle structures and loading/releasing properties of payloads, leading to the development of useful strategies for designing and tailoring pharmaceutical and biomedical nanomaterials.

Here, we report the aqueous onion-like vesicles of PEO-*b*-PCL prepared by emulsification/solvent-evaporation (referred to as the emulsification-induced assembly hereafter, **Figure 1**). Although the in situ self-assembly of PEO-*b*-PCL showed a strong tendency to form nanofibrils, regardless of a variation in the relative block weight ratios and total molecular weights, the emulsification-induced assembly generates helical ribbons, tubules, and unique vesicles through the packing modification of the semicrystalline PCL core. In particular, the presence of multi-walls separated by water channels containing the hydrated PEO chains within a single vesicular system, in contrast to concentric multi-walled vesicles,[27,28] was confirmed by 3D cryogenic-electron tomography (cryo-ET).[29,30] The formation of multicompartmentalized vesicle stimulated us to investigate their specific capability for the loading of therapeutic drugs and/or diagnostic imaging agents within the hydrophobic walls. Remarkably, the onion-like vesicles, with a high-ordered feature, exhibited higher drug-loading capacity and stepwise drug-releasing behavior via hydrolytic degradation of the walls compared to that observed with the single-walled vesicular hybrids, containing inorganic imaging nanoagents, and in situ self-assembled fibrils constructed using the same PEO-*b*-PCL polymer.

2. Results and Discussion

2.1. Fibrillar Association of PEO-*b*-PCL by In Situ Self-Assembly

The nanoaggregates of PEO-*b*-PCL amphiphiles were first prepared via the in situ self-assembly method (**Scheme 1**). PEO_{1K}-*b*-PCL_{1K}, PEO_{1K}-*b*-PCL_{5K}, and PEO_{5K}-*b*-PCL_{5K} were employed and dissolved in aqueous solution (1.0 mg mL^{-1}, Table S1, Supporting Information) to investigate whether a variation in the relative block weight ratios and total molecular weights affects the morphology of self-aggregate.

Transmission electron microscopy (TEM) image of PEO_{1K}-*b*-PCL_{1K} showed the formation of micrometer-long fibrils with a regular diameter of 11.4 ± 0.7 nm (**Figure 2**a and Figure S1a, Supporting Information). In general, the increase in the length of hydrophobic block in the amphiphilic diblock copolymer architecture results in the reduction of interfacial curvature between hydrophobic and hydrophilic regions in aqueous solution, leading to the structural transformation from cylinders to layered structures such as sheets and vesicles.[31,32] Nevertheless, PEO_{1K}-*b*-PCL_{5K} with an increase in the molecular weight of PCL block up to fivefold also formed fibrils (Figure S1b, Supporting Information). Even when increasing the molecular weight of each block up to 5 kDa (PEO_{5K}-*b*-PCL_{5K}), the fibrillar nature was retained (Figure S1c, Supporting Information). Interestingly, the selected area electron diffraction (SAED) patterns of all resulting fibrils revealed the (110) and (200) reflections, corresponding to the orthorhombic PCL crystals located in the fibril core (Figure S1d–f, Supporting Information).[33,34]

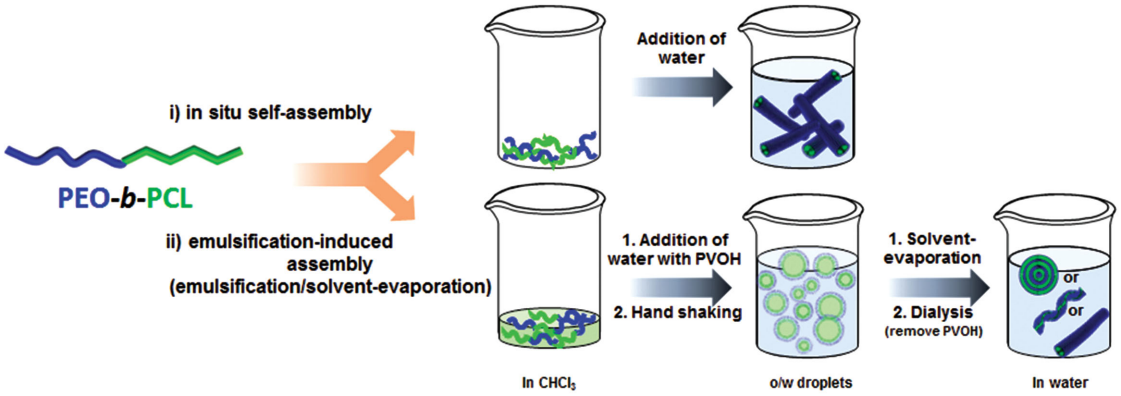

Scheme 1. Schematic illustration showing the "in situ self-assembly" and "emulsification-induced assembly" methods for the preparation of nanostructured particles of PEO-*b*-PCL.

2.2. Emulsification-Induced Assembly of PEO-*b*-PCL into Various Nanostructures

The strong propensity of a series of PEO-*b*-PCLs to form fibrils with crystalline features was affected by emulsification-induced assembly (Scheme 1).[23–25] The chloroform solution of block copolymer was easily emulsified manually in water with the presence of polyvinyl alcohol (PVOH) as a surfactant to prepare the oil-in-water (o/w) droplets. Upon gradual removal of the chloroform, the increased concentration of PEO-*b*-PCL within the droplets led the polymer migration to the oil–water interface, spontaneously resulting in the corrugation of droplet surface (Figure 2b and Figure S2, Supporting Information).[23–26] It has been reported that such interfacial instability could be driven by a reduction of the interfacial tension, triggering the ejection of tiny droplets or interfacial roughening.[35] Indeed, both PEO_{1K}-*b*-PCL_{1K} and PEO_{5K}-*b*-PCL_{5K} droplets with a PEO weight fraction of 0.50 ejected the smaller droplets into the aqueous phase. No aggregates were eventually observed in the optical micrographs. However, when the weight fraction of PEO was decreased to 0.17 (PEO_{1K}-*b*-PCL_{5K}), microspheres were observed in optical micrographs, which resulted from the shrinkage of mother droplets along with the collapse of the ejected smaller droplets (Figure S2b, Supporting Information).

Interestingly, these distinguishable behaviors between the o/w droplets of PEO-*b*-PCLs upon solvent-evaporation triggered the different morphologies of the resulting aggregates. Although the emulsification-induced assembly of PEO_{1K}-*b*-PCL_{1K} formed nanofibrils similar to those obtained by in situ self-assembly, the fibril diameter increased from 11.4 ± 0.7 nm up to 14.4 ± 1.6 nm (Figure 2c and Figure S3a, Supporting Information). The SAED pattern of fibrils revealed the noticeable reduction of PCL crystallinity compared to that of self-assembled fibrils (Figure 2c). Therefore, the increased fibril diameter could be explained by the increment of amorphous contents of PCL within the core in compensation for the reduction of close-packed arrangements of PCL contributing to its crystalline nature. Strikingly, PEO_{5K}-*b*-PCL_{5K} droplets generated predominantly helical ribbons (**Figure 3**). The somewhat tubular structures were observed in both TEM (Figure 3i) and cryo-TEM images (Figure 3j). Since inevitable solvent-evaporation for the preparation of conventional TEM specimen often causes the morphological transition of solution-state aggregates or artifacts,[29] cryo-TEM experiments were conducted. The TEM results suggest that tubules with a different diameter originated from the elemental ribbons with a diverse helical pitch. We speculate that the formation of helical ribbons by an increase in the molecular weight of both the PCL core and corona-forming PEO chains[36,37] might be explained by the

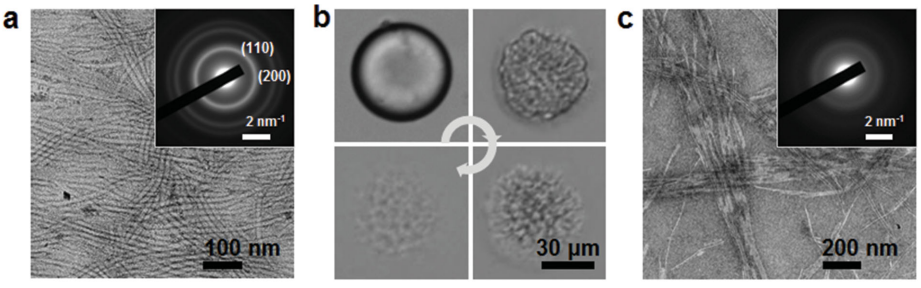

Figure 2. Fibrillar association by in situ self-assembly versus emulsification-induced assembly. a) Negatively stained TEM image of fibrils formed from the self-assembly of PEO_{1K}-*b*-PCL_{1K} in aqueous solution (with a 2 wt% uranyl acetate solution; inset, SAED pattern of fibrils). b) Optical micrographs showing the solvent-evaporation process (clockwise from top left) of o/w-emulsion droplet of PEO_{1K}-*b*-PCL_{1K}. c) Negatively stained TEM image of fibrils formed by emulsification-induced assembly of PEO_{1K}-*b*-PCL_{1K} (inset, SAED pattern of fibrils).

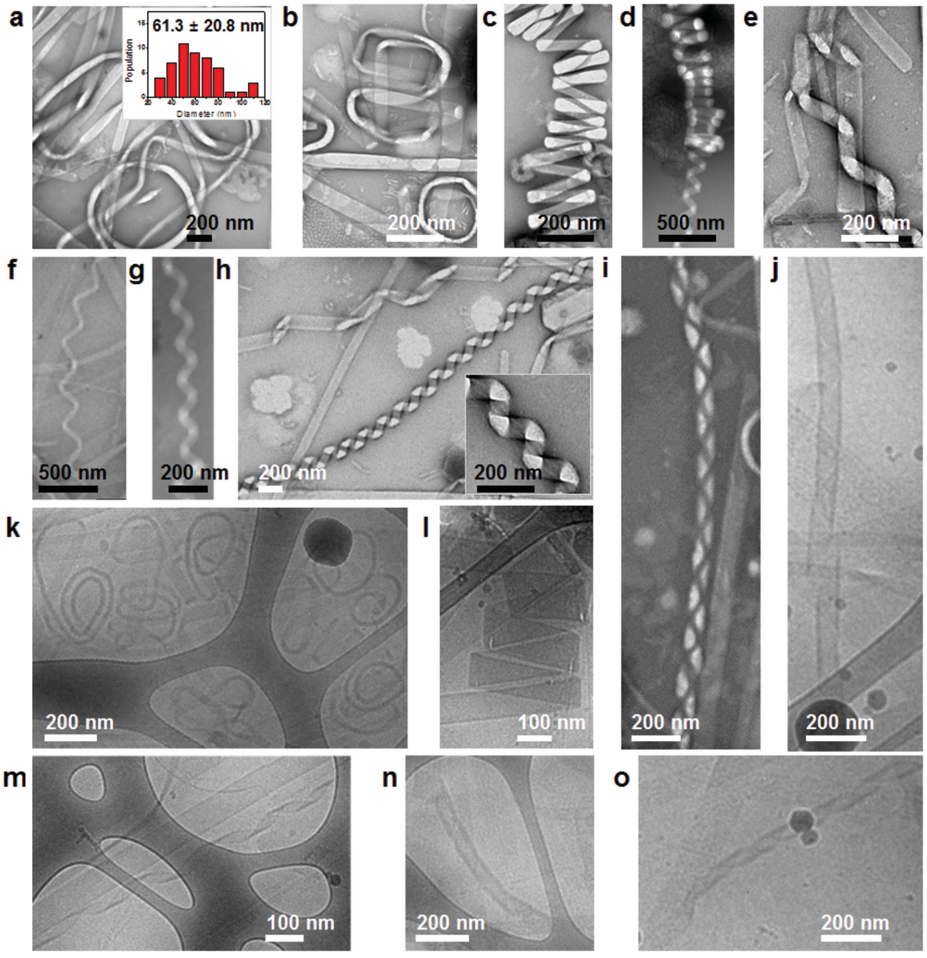

Figure 3. Helical ribbons and tubules generated by emulsification-induced assembly of PEO_{5K}-*b*-PCL_{5K}. a–i) Negatively stained TEM and j–o) cryo-TEM images showing the morphological transition from flat ribbons to helical ribbons and then to tubules.

spatial tilted arrangements of polymers, arising from the combination of enhanced hydrophobic interaction of the PCL block with crystalline nature and an increased steric crowding between the neighboring PEO chains in a 1D way.[37] To our knowledge, this is the first observation of helical nanoribbons generated from PEO-*b*-PCL assembly.

More interestingly, the solvent-evaporation of the PEO_{1K}-*b*-PCL_{5K} o/w droplets gave rise to the so-called "onion-like vesicles" containing multi-walls along with microparticles. A wall thickness of 21.3 ± 3.0 nm was determined from the TEM image (**Figure 4**a). In the course of the TEM experiments confirming the structure of aggregates after solvent evaporation, some budding particles were captured (Figure S4, Supporting Information), which probably were intermediate states. The bud protrusions studded at the rim of the particle are composed of multilayer. Therefore, the onion-like vesicles seem to be generated from buds. To exclude the effects of the initial droplet size and/or the rate of solvent-removal on the morphologies of resulting nanoparticle,[26] the monodisperse emulsion droplets of PEO_{1K}-*b*-PCL_{5K}, with a diameter of approximately 40 µm, were prepared by using a glass capillary fluidic device (Figure 4b).[38] The onion-like vesicles, up to a few hundred nanometers in diameter, were successfully regenerated (Figure S3b, Supporting Information). Spherical microparticles with a regular diameter of approximately 8 µm were easily separated from the vesicles by simple filtration through a membrane filter with a pore size of 0.8 µm (Figure S3c, Supporting Information), which was confirmed by dynamic light scattering (DLS) experiments (Figure S5, Supporting Information).

2.3. 3D Structural Elucidation of Onion-Like Vesicles

The cryo-TEM image of PEO_{1K}-*b*-PCL_{5K} solution showed the existence of multilamellar capsules against the vitrified solution background, in which there is considerable spacing between the walls (Figure 4c). The wall thickness and the spacing between the walls were 17.5 ± 2.2 nm and 16.2 ± 4.3 nm, respectively (Figure S6, Supporting Information).[39] Details of the 3D structure of onion-like vesicles were studied by tomography using TEM and cryo-TEM (**Figure 5** and Movie 1-4, Supporting Information). A series of 2D images of the same object taken at various tilt angles was merged and fully aligned to create a 3D nanostructure by using a weighted

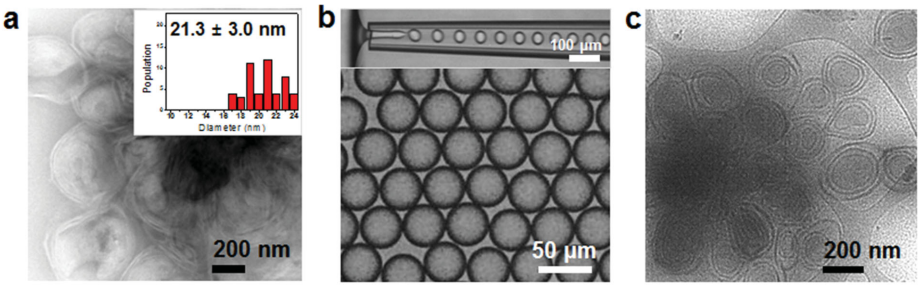

Figure 4. a) Negatively stained TEM image of onion-like vesicles of PEO_{1K}-*b*-PCL_{5K} (inset, the size distribution graph of wall thickness). b) Optical photographs showing the monodisperse o/w-emulsion droplets of PEO_{1K}-*b*-PCL_{5K} generated by glass capillary fluidic device. c) Cryo-TEM image of onion-like vesicles.

back-projection algorithm (Figure S7, Supporting Information). Since the total tolerable electron dose for tilt series and the attainable resolution should be compromised to avoid radiation damage of organic PEO-*b*-PCL sample from the electron beam, a total of 137 and 27 images were recorded by TEM and cryo-TEM at various tilt angles from −68° to +68° and −39° to +39° with increments of 1° and 3°, respectively. The low contrast of tomogram was improved by filtering to enhance visualization. In each tomographic slice, the inner and outer walls were drawn by computer-assisted tracking of high contrast lines. When all drawn lines were combined, a 3D volume model was generated (Figure 5a,c). Detailed analysis from 3D reconstructed volume of vesicles indicated the number of walls in a single vesicle (Figure 5b,d). Additionally, there was

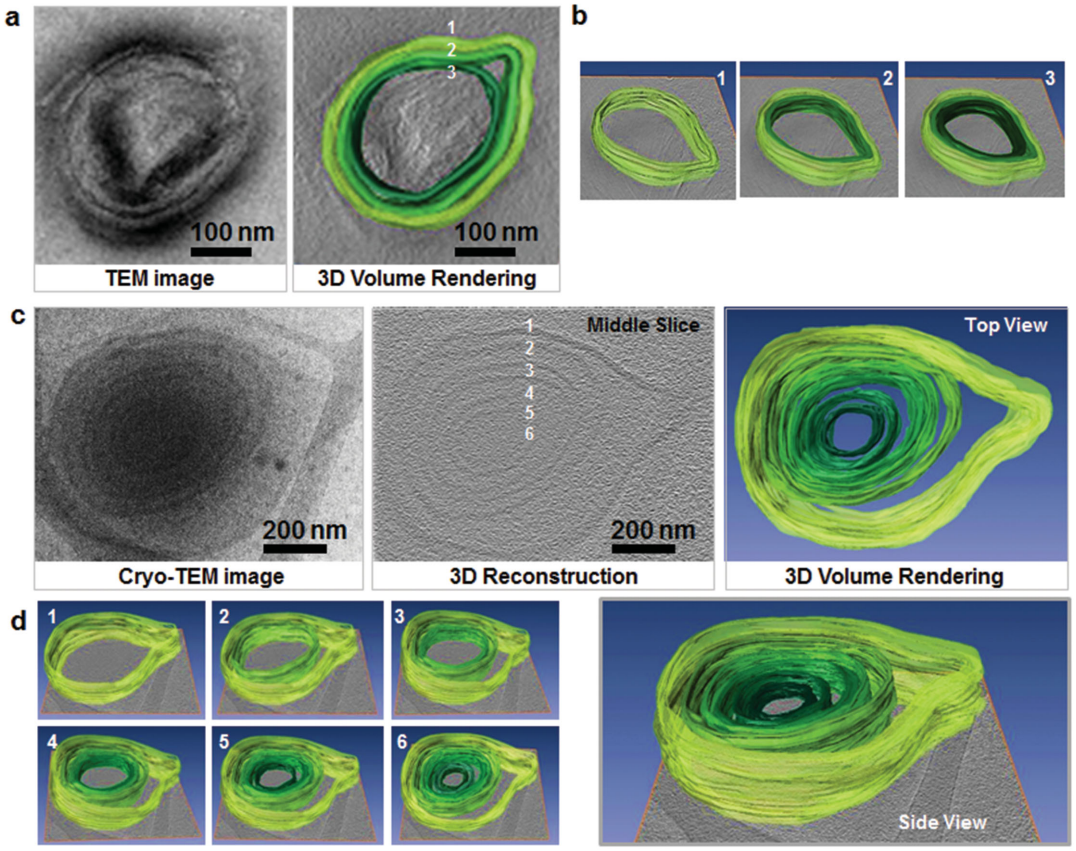

Figure 5. 3D structural elucidation of onion-like vesicles with water channels. a–d) Electron-tomography (ET) reconstruction of onion-like vesicles. a, left) Conventional TEM image and a, right; b) reconstructed 3D volume of onion-like vesicles. b) Sequential drawing from the outermost to innermost wall is represented. c) Cryo-ET reconstruction of vitrified onion-like vesicles. c,d) Reconstructed image and 3D volume data showing the multi-walled vesicles with water channels.

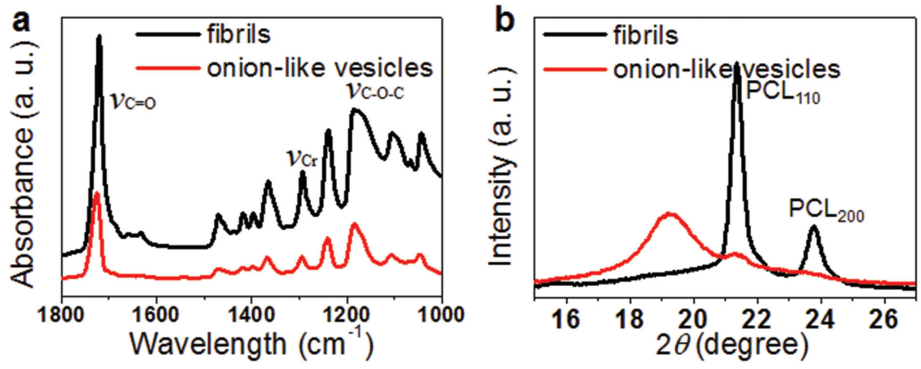

Figure 6. a) ATR-FTIR spectrum and b) WAXS data of self-assembled fibrils and emulsification/solvent-evaporation induced onion-like vesicles of PEO_{1K}-*b*-PCL_{5K}.

no interconnection between the walls. Especially, cryo-ET of vitrified onion-like vesicles further demonstrated that the space between the walls is filled with water in contrast to the concentric multilamellar vesicles (Figure 5c).[27] It should be noted that the dried onion-like vesicles looked like concentric vesicles, containing no spaces between the walls (Figure 5a). Generally, in cryo-TEM images, hydrophobic PCL cores appeared dark, whereas the solvated PEO was not directly visible.[27,39] Considering the wall thickness of 21.3 ± 3.0 nm, observed in TEM, the wall thickness and the distance between the walls of 17.5 ± 2.2 nm and 16.2 ± 4.3 nm, respectively, indicate the presence of a water channel containing the hydrated PEO chains. This unique structural feature of the vesicle contributes to it being considered as an effective nanovehicle, having alternating compartments for both hydrophilic and hydrophobic chemical species.

This morphological transition of PEO_{1K}-*b*-PCL_{5K} from fibrils to onion-like vesicles, induced by changing from in situ self-assembly to emulsification-induced assembly, can be understood by the reduction of the crystalline feature of PCL block, as mentioned previously. The SAED pattern of onion-like vesicles did not reveal the strong semicrystalline characteristic of PCL block (Figure S8, Supporting Information). Further evidence was acquired by attenuated total reflection-Fourier transform infrared (ATR-IR) spectroscopy, which monitors C═O, C—C and symmetrical C—O—C stretching vibrations of PCL (**Figure 6**a).[40] In the spectra of 1000–1800 cm^{-1} region of self-assembled fibrils, the strong absorption bands peaked at 1721 cm^{-1} for $\nu_{C=O}$, at 1293 cm^{-1} for ν_{cr}, and at 1183 cm^{-1} for ν_{C-O-C} (Table S2, Supporting Information). When replaced with the onion-like vesicles, $\nu_{C=O}$ at 1721 cm^{-1} shifted to a higher wavenumber (1726 cm^{-1}), which means that amorphous character of PCL increased.[40] In addition, the wide-angle X-ray scattering (WAXS) measurement of the film cast from the aqueous fibril solution showed two strong reflections of (110) and (200) of PCL at $2\theta = 21.3°$ and 23.8° (Figure 6b), which originated from the highly ordered and chain folding characteristics, indicating the existence of the crystalline characteristic of PCL.[41] By modifying the sample from fibrils to onion-like vesicles, the intensity of two characteristic peaks of crystalline PCL was suppressed, while the amorphous halo increased. These results indicated that the aqueous self-assembled nanostructure of PEO-*b*-PCL has a more crystalline PCL core than do the emulsification-induced onion-like vesicles, resulting in the formation of 1D rigid fibrillar structure.

2.4. Encapsulation of Doxorubicin and Magnetite Iron Oxide Nanoparticles

To investigate the encapsulation ability of onion-like vesicles for biomedical delivery applications,[42] Nile red was employed as a simple hydrophobic drug model. The fluorescence micrograph of o/w emulsion of PEO_{1K}-*b*-PCL_{5K} showed the preservation of stable droplets after addition of Nile red (**Figure 7**a). After evaporation of chloroform, the onion-like vesicles were obtained without any structural changes (Figure 7b). Nile red emission, restricted in vesicle, appeared at a lower wavelength (622 nm) compared to that of other polymers (627 nm, Figure 7c), which is strongly influenced by its environment polarity.[43] It can be concluded that Nile red was closely packed within the PEO_{1K}-*b*-PCL_{5K} vesicle walls through strong hydrophobic interactions.

The formation of onion-like vesicle of PEO_{1K}-*b*-PCL_{5K} even after encapsulating the Nile red led us to fabricate multifunctional vesicles through the additional incorporation of iron oxide nanoparticles (Fe_3O_4 NPs) into the wall. Doxorubicin (Dox) and Fe_3O_4 NPs were selected as a representative anticancer drug and a diagnostic imaging agent, respectively. The o/w emulsion droplets of PEO_{1K}-*b*-PCL_{5K} containing Dox and oleic acid-stabilized Fe_3O_4 NPs with a diameters of 3.6 ± 0.5 nm (Figure S9, Supporting Information) were stable and moved along the external magnetic field in aqueous solution (Figure S10, Supporting Information). Unfortunately, the resulting nanoparticles after removal of chloroform were structurally transformed. Single-walled nanovesicles were formed, with the microscale multivesicular vesicles containing several small vesicles (Figure 7d). All vesicles seemed to be covered with Fe_3O_4 NPs, as shown in the TEM image (Figure 7e). However, the cross-sectional view of the hybrid vesicles shows that Fe_3O_4 NPs are arranged in a single-layered, circular manner (Figure 7f). The appearance of Dox emission in the aqueous solution indicated

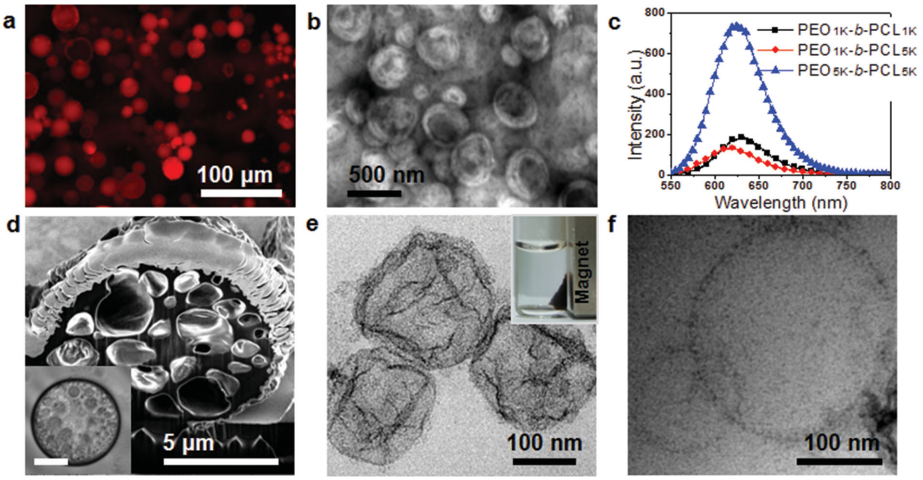

Figure 7. Entrapment of drugs and magnetic iron oxide NPs by emulsification-induced assembly. a) Fluorescence micrograph of o/w-emulsion droplets of PEO_{1K}-*b*-PCL_{5K} containing Nile red (λ_{ex} = 530 nm). b) TEM image of onion-like vesicles formed by solvent-evaporation of PEO_{1K}-*b*-PCL_{5K} emulsion droplets containing Nile red. c) Fluorescence spectra showing the Nile red-encapsulation capability of aqueous nanostructures of PEO-*b*-PCLs. d) Optical micrograph of an emulsion droplet of PEO_{1K}-*b*-PCL_{5K} containing Fe_3O_4 NPs and Dox (inset, scale bar of 25 μm), and the cross-sectional SEM image of a multivesicular vesicle, generated from the solvent-evaporation of o/w droplet. e) Hybrid vesicles of PEO_{1K}-*b*-PCL_{5K} formed by simultaneous encapsulation of Fe_3O_4 NPs and Dox (inset of (e), photographs of droplets with an external magnetic field). f) Ultramicrotomed films of hybrid vesicles showing the arrangement of Fe_3O_4 NPs.

that Dox was well-intercalated simultaneously with Fe_3O_4 NPs in the vesicle walls to avoid the unfavorable contacts between the hydrophobic part and water (Figure S11, Supporting Information).[11,44] The quantity of Fe_3O_4 NPs loaded within the walls was measured to be 6 wt% by thermogravimetric analysis (TGA, Figure S13, Supporting Information). Note that both PEO_{1K}-*b*-PCL_{1K} and PEO_{5K}-*b*-PCL_{5K} droplets containing Dox and Fe_3O_4 NPs also formed single-walled vesicles. This tendency can be rationalized by the large entropic cost of inserting NPs with a large volume into a PCL domain and the subsequent frustration of regular packing of PCL.[44] A paramount increase in the volume of the hydrophobic part affects the curvature of the wall, leading to the morphological change into the vesicles.

2.5. Stepwise Drug-Release Behavior of Onion-Like Vesicles

The nanostructural diversity of PEO_{1K}-*b*-PCL_{5K}, observed upon loading of drugs or both drugs and imaging agents, triggers different drug-releasing behaviors through the competitive dissociation of vehicles attributed to the hydrolytic cleavage of PCL.[45] Dox-loading/releasing abilities of self-assembled fibrils, onion-like vesicles, and single-walled vesicular hybrids containing Fe_3O_4 NPs of PEO_{1K}-*b*-PCL_{5K} were compared. We expected that the onion-like vesicles would present an increase in the hydrophobic drug capacity, a prolonged circulation time in the blood, and exhibit long-lasting drug release due to its multi-walled nature.[46] The drug loading contents (DLC) of Dox were determined by fluorescence measurement (λ_{ex} = 470 nm, Figure S14, Supporting Information).[47] The theoretical DLCs were set to be 9.1 wt%. The actual DLCs of onion-like vesicles, fibrils, and single-walled vesicular hybrids were 7.5%, 6.3%, and 5.3%, respectively (**Figure 8**a). As expected, onion-like vesicles showed a higher DLC value than other structures. The aqueous vesicle composed of multi-walls allows a greater volume for hydrophobic payloads in confined spaces. The achieved drug loading efficiency (DLE) of onion-like vesicles was also the highest (89.6%) among the nanostructures (Figure 8a).

The in vitro Dox-release studies of nanocarriers were carried out under pH 7.4 at 37 °C.[48,49] The Dox-release was boosted at pH 5.5, corresponding to the acidic environment inside tumor tissue and endolysosomal compartments of tumor cells. The destructed hydrophobic interactions between Dox and PCL blocks by both reprotonation of amino group of Dox and faster cleavage of ester bonds in PCL core, under acidic conditions, resulted in the increased water solubility of Dox.[50]

A free Dox solution was treated as a control and was fully released in 8 h, while Dox within vehicles exhibited a more sustained release (Figure 8b). In both fibril and single-walled hybrid vesicle solutions, a two-phase release profile was observed. First, Dox-release was relatively rapid for 12 h followed by a gradual decrease in the release rate over several weeks. The cumulative Dox-release amounts from fibrils and hybrid vesicles of PEO_{1K}-*b*-PCL_{5K} reached up to 37% and 33%, respectively, in the first 12 h, and then to 74% and 60% over a 24-d period, respectively. SAED pattern of Dox-loaded fibrils showed the existence of PCL crystalline feature, while that of Dox-loaded hybrid vesicles revealed no PCL crystallinity (Figure S15, Supporting Information). Since the chemical compatibility between the drugs incorporated in the core and core-forming block is an important factor determining drug-release rates,[51] these results could be explained by the hypothesis that more densely packed PCL, consisting of mainly aliphatic polyesters, forms the microchannel structure within the fibrillar core,[52] causing a faster exposure and release of Dox containing aromatic rings to the aqueous media.

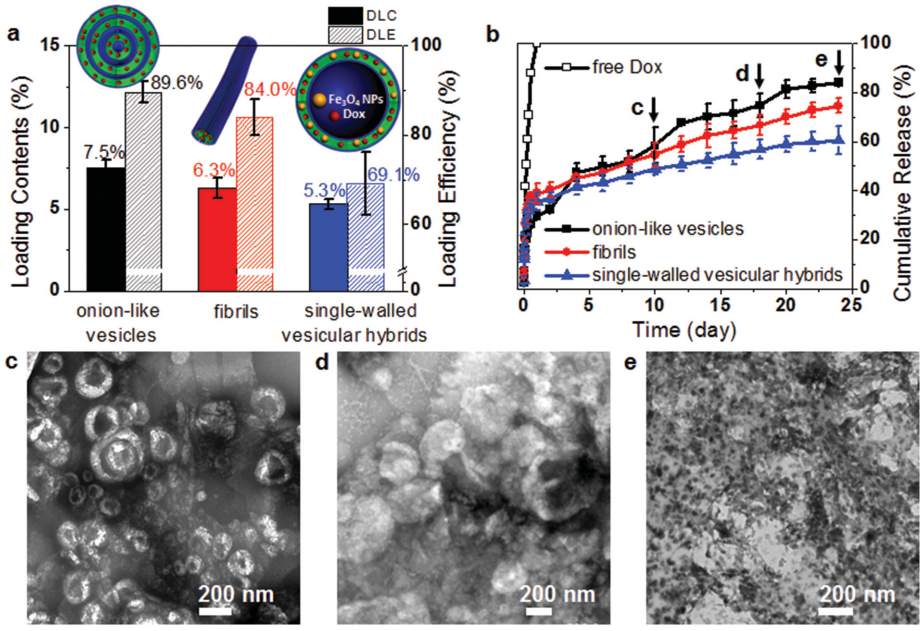

Figure 8. a) Drug loading content (DLC) and efficiency (DLE) for Dox-loaded onion-like vesicles, fibrils and single-walled vesicular hybrids of PEO_{1K}-*b*-PCL_{5K} (red and orange spheres in schematic illustration indicating Dox and Fe_3O_4 NPs, respectively). b) In vitro release of free Dox and nanostructures of PEO_{1K}-*b*-PCL_{5K} in acetate buffer of pH 5.5 at 37 °C using membrane dialysis procedure over 24 d. All data points presented are average values of three replicate experiments and error bars indicate standard deviations. TEM images showing morphological transition of onion-like vesicles as drug-release proceeds; after c) 10 d, d) 18 d, and e) 24 d.

Remarkably, onion-like vesicles showed the stepwise drug-releasing characteristic. Although 84% of Dox was released over 24 d, four stages of Dox-release were observed (Figure 8b). It would be attributed to the gradational degradation of vesicles from the outermost to innermost walls. TEM measurements showed that onion-like vesicles decomposed into single-walled vesicles, which, in turn, led to the shapeless aggregates over time (Figure 8c–e). Therefore, it is expected that a greater amount of Dox-loaded walls of vesicle could remain for a considerable period in the plasma after intravenous administration even though premature drug release occurred upon erosion of the polymer nanovehicle. Many different parameters that contribute to the complicated release process sometimes play a contradictory role. However, considering the requirements for clinical application, including properties such as high DLC and DLE, long blood circulation time, and long-lasting drug release, the onion-like vesicles are the best carriers among the nanostructures of PEO-*b*-PCL fabricated in this study.

3. Conclusion

The aqueous onion-like vesicles of PEO-*b*-PCL with a simple linear architecture, containing water channels between the walls, were fabricated. Although the in situ self-assembly of PEO-*b*-PCLs showed the formation of nanofibrils, the emulsification-induced assembly generates unique nanostructures, such as helical ribbons, tubules, and onion-like vesicles, through the packing modification of PCL core. The crystallinity control of PCL block at the molecular scale significantly affects not only the spatial organization of the aggregates at the nanoscale but also the subsequent loading/releasing of payloads. In particular, the detailed ultrastructure of onion-like vesicles was interpreted by integrating the 3D electron microscopic analysis. The multi-walled nature and the sequential hydrolytic PCL cleavage from the outermost to innermost walls led to a higher drug-loading efficiency and stepwise drug release, respectively, which enable us to envision their great potential for prolonging drug-retention time in blood circulation. The multifunctional vehicles were also successfully prepared by incorporating therapeutic and diagnostic agents into the wall, even though the morphology was altered from multi-walled to single-walled vesicles. Therefore, the exquisite fabrication of unique and complex nanostructure and study of its correlation with drug delivery properties would be a paramount subject, which further provides a useful strategy for developing and fine-tuning the functionalities of organic and organic–inorganic hybrid nanomaterials in biomedical applications.

4. Experimental Section

Loading of Dox into Nanostructures, Including Onion-Like Vesicles, Vesicles, and Fibrils: For the in situ self-assembly method, 100 μL of PEO-*b*-PCL (10 mg mL^{-1} in chloroform) and 10 μL of Dox (10 mg mL^{-1} in chloroform) were mixed, and the solvent was then evaporated, followed by addition of 1 mL of water. The feed weight ratio of copolymer to drug was fixed at 10:1. The unloaded Dox was removed by centrifugation (13.5 krpm for 15 min) before lyophilization. The Dox-loaded nanoparticles were redissolved in 1 mL of water. For the emulsification-induced assembly method, 100 μL of PEO-*b*-PCL (10 mg mL^{-1} in

chloroform) and 10 μL of Dox (10 mg mL^{-1} in chloroform) were added to 1 mL of water containing PVOH and then mixed manually. The feed weight ratio of the copolymer to the drug was fixed at 10:1. Unloaded Dox, chloroform, and PVOH were removed by dialysis against water for 48 h using a dialysis membrane (MWCO, 14 kDa), followed by centrifugation (13.5 krpm for 15 min). In particular, the resultant nanoparticles such as onion-like vesicles and microparticles were separated by filtration using a membrane filter with a pore size of 0.8 μm. The Dox-loaded nanoparticles were redissolved in 1 mL of water. Fe_3O_4 NPs/Dox co-loaded vesicle was prepared by using 100 μL of PEO-*b*-PCL (10 mg mL^{-1} in chloroform), 10 μL of Fe_3O_4 NPs (1 mg mL^{-1} in chloroform), and 10 μL of Dox (10 mg mL^{-1} in chloroform). The following procedures were same as described previously.

In Vitro Drug Release Study: The Dox-release from the Dox-loaded nanostructure was conducted in dialysis tube (in 1 mL), which was suspended in 20 mL of acetate buffer (50×10^{-3} M, pH 5.5) at 37 °C with constant shaking at 100 rpm. At certain time intervals, 1 mL of the dialysis membrane was emptied and replenished with the same volume of fresh medium. At the completion of the study, Triton X-100 solution was added to the nanostructure solution and fluorescence was determined. The amount of released Dox was measured by fluorescence spectrometry (λ_{ex} = 470 nm, emission range from 500 to 800 nm) and the cumulative release curve of Dox was obtained. The release experiments were performed in triplicate under the dark.

Transmission Electron Microscopy: A drop of each sample in aqueous solution was placed on a formvar/carbon-coated copper grid and allowed to evaporate under ambient conditions. When the sample was stained, a drop of uranyl acetate solution (2 wt%) was placed onto the sample-loaded grid. The specimen was observed with a JEM-3011 HR (JEOL, Japan), operating at 300 kV, and a JEM-1400 (JEOL), operating at 120 kV.

TEM Tomography: 3D reconstruction of vesicles obtained from a series of 2D image projections of the samples at different viewing angles. For TEMT, images were obtained using a JEM-2100F (JEOL), operating at 200 kV, and a charge-coupled device (CCD) camera size of 2048 × 2048 (Gatan, USA). In total, 137 images were acquired at tilting angles between −68° and 68°, with an increment of 1°. The magnification was 8000×, corresponding to a pixel size of 2.42 nm. Tilting, refocusing, and repositioning were carried out after every individual tilt increase. Alignment and reconstruction of tilt series (100 slices of 4.8 nm thickness each were obtained) were performed in IMOD software. Amira 5.5 software was used for visualization.

Cryogenic Transmission Electron Microscopy (cryo-TEM): The cryo-TEM experiments were performed with a thin film of aqueous sample solution (5 μL) transferred to a lacey supported grid by the plunge-dipping method. The thin aqueous films were prepared at ambient temperature and with a humidity of 97%–99% within a custom-built environmental chamber in order to prevent water evaporation from the sample solution. The excess liquid was blotted with filter paper for 1–2 s, and the thin aqueous films were rapidly vitrified by plunging them into liquid ethane (cooled by liquid nitrogen) at its freezing point. The specimen was observed with a JEM-3011 HR, operating at 300 kV.

Cryo-Electron Tomography: The samples were prepared as described for cryo-TEM. The specimen was observed with a Tecnai G2 (FEI, USA), operating at 120 kV and a CCD camera full resolution of 2048 × 2048 pixels (Gatan). Tilt series were recorded under low-dose conditions (total electron dose of <150 eÅ^{-2}) by collecting images between −39° and 39°, with an increment of 3°. The defocus was set to −3.74 μm. The pixel size of projections was 0.98 nm. A series of images for alignment and reconstruction was obtained using the IMOD software. After reconstruction, 200 slices of 2.0 nm thickness each were obtained. 3D visualization of the volume data was performed using the Amira 5.5 software.

Supporting Information

Supporting Information is available from the Wiley Online Library or from the author.

Acknowledgements

M.-K.P. and S.J. contributed equally to this work. This research was supported by Basic Science Research Program (2013R1A1A2061197, 2013R1A2A2A04015914) through the National Research Foundation of Korea (NRF) funded by the Korea Government (MEST), the Korea Basic Science Institute grant (T34430), and Chungnam National University Research Fund. Experiments at PLS (Beamline 9A) were supported in part by MSIP and POSTECH.

Received: April 20, 2015
Revised: May 31, 2015
Published online: June 18, 2015

[1] Y. Mai, A. Eisenberg, *Chem. Soc. Rev.* **2012**, *41*, 5969.
[2] R. C. Hayward, D. J. Pochan, *Macromolecules* **2010**, *43*, 3577.
[3] K. Letchford, H. Burt, *Eur. J. Pharm. Biopharm.* **2007**, *65*, 259.
[4] G. Gaucher, M.-H. Dufresne, V. P. Sant, N. Kang, D. Maysinger, J.-C. Leroux, *J. Controlled Release* **2005**, *109*, 169.
[5] A. Rösler, G. W. M. Vandermeulen, H.-A. Klok, *Adv. Drug Delivery Rev.* **2012**, *64*, 270.
[6] H. Otsuka, Y. Nagasaki, K. Kataoka, *Curr. Opin. Colloid Interface Sci.* **2001**, *6*, 3.
[7] N.-V. Cuong, J.-L. Jiang, Y.-L. Li, J.-R. Chen, S.-C. Jwo, M.-F. Hsieh, *Cancers* **2011**, *3*, 61.
[8] F. Wang, T. K. Bronich, A. V. Kabanov, R. D. Rauh, J. Roovers, *Bioconjugate Chem.* **2005**, *16*, 397.
[9] M. Antonietti, S. Förster, *Adv. Mater.* **2003**, *15*, 1323.
[10] D. A. Christian, S. Cai, D. M. Bowen, Y. Kim, J. D. Pajerowski, D. E. Discher, *Eur. J. Pharm. Biopharm.* **2009**, *71*, 463.
[11] J. Jang, J.-K. Kim, J.-W. Choi, T.-S. Hwang, M. Jo, I. Kim, B.-K. Cho, E. Lee, *Chem. Commun.* **2013**, *49*, 8003.
[12] I. Mellman, *Annu. Rev. Cell Dev. Biol.* **1996**, *12*, 575.
[13] G. Schmitz, G. Müller, *J. Lipid Res.* **1991**, *32*, 1539.
[14] D. L. Sherman, P. J. Brophy, *Nat. Rev. Neurosci.* **2005**, *6*, 683.
[15] A. B. Novikoff, *Proc. Natl. Acad. Sci. U.S.A.* **1976**, *73*, 2781.
[16] M. Marguet, C. Bonduelle, S. Lecommandoux, *Chem. Soc. Rev.* **2013**, *42*, 512.
[17] S. Mitragotri, J. Lahann, *Nat. Mater.* **2009**, *8*, 15.
[18] G. Rizis, T. G. M. van de Ven, A. Eisenberg, *Angew. Chem. Int. Ed.* **2014**, *53*, 9000.
[19] Y. Geng, P. Dalhaimer, S. Cai, R. Tsai, M. Tewari, T. Minko, D. E. Discher, *Nat. Nanotechnol.* **2007**, *2*, 249.
[20] R. Vácha, F. J. Martinez-Veracoechea, D. Frenkel, *Nano Lett.* **2011**, *11*, 5391.
[21] R. Vácha, F. J. Martinez-Veracoechea, D. Frenkel, *ACS Nano* **2012**, *6*, 10598.
[22] P. Alexandridis, B. Lindman, *Amphiphilic Block Copolymers: Self-Assembly and Applications* Elsevier, Amsterdam **2000**.
[23] J. Zhu, R. C. Hayward, *J. Am. Chem. Soc.* **2008**, *130*, 7496.
[24] J. Zhu, R. C. Hayward, *Angew. Chem. Int. Ed.* **2008**, *47*, 2113.
[25] S. Liu, R. Deng, W. Li, J. Zhu, *Adv. Funct. Mater.* **2012**, *22*, 1692.
[26] I. Wyman, G. Njikang, G. Liu, *Prog. Polym. Sci.* **2011**, *36*, 1152.
[27] S. Zhang, H.-J. Sun, A. D. Hughes, R.-O. Moussodia, A. Bertin, Y. Chen, D. J. Pochan, P. A. Heiney, M. L. Klein, V. Percec, *Proc. Natl. Acad. Sci. U.S.A.* **2014**, *111*, 9058.
[28] J.-L. A. N. Murk, M. N. Lebbink, B. M. Humbel, W. J. C. Geerts, J. M. Griffith, D. M. L. Langenberg, F. A. W. Verreck, A. J. Verkleij, A. J. Koster, H. J. Geuze, M. J. Kleijmeer, *Traffic* **2004**, *5*, 936.
[29] H. Friedrich, P. M. Frederik, G. de With, N. A. J. M. Sommerdijk, *Angew. Chem. Int. Ed.* **2010**, *49*, 7850.
[30] L. Bonetta, *Nat. Methods* **2005**, *2*, 139.
[31] S. Jain, F. S. Bates, *Science* **2003**, *300*, 460.
[32] S. J. Holder, N. A. J. M. Sommerdijk, *Polym. Chem.* **2011**, *2*, 1018.

[33] Z.-X. Du, J.-T. Xu, Z.-Q. Fan, *Macromolecules* **2007**, *40*, 7633.
[34] J. Sun, X. Chen, C. He, X. Jing, *Macromolecules* **2006**, *39*, 3717.
[35] R. Granek, R. C. Ball, M. E. Cates, *J. Phys. II* **1993**, *3*, 829.
[36] G. Battaglia, A. J. Ryan, *Macromolecules* **2006**, *39*, 798.
[37] E. Lee, B. Hammer, J.-K. Kim, Z. Page, T. Emrick, R. C. Hayward, *J. Am. Chem. Soc.* **2011**, *133*, 10390.
[38] A. S. Utada, E. Lorenceau, D. R. Link, P. D. Kaplan, H. A. Stone, D. A. Weitz, *Science* **2005**, *308*, 537.
[39] E. Lee, J.-K. Kim, M. Lee, *Macromol. Rapid Commun.* **2010**, *31*, 975.
[40] B. Zhu, J. Li, Y. He, N. Yoshie, Y. Inoue, *Macromol. Biosci.* **2003**, *3*, 684.
[41] F. Xue, X. Chen, L. An, S. S. Funari, S. Jiang, *Polym. Int.* **2012**, *61*, 909.
[42] P. P. Ghoroghchian, P. R. Frail, K. Susumu, D. Blessington, A. K. Brannan, F. S. Bates, B. Chance, D. A. Hammer, M. J. Therien, *Proc. Natl. Acad. Sci. U.S.A.* **2005**, *102*, 2922.
[43] B. Karagoz, C. Boyer, T. P. Davis, *Macromol. Rapid Commun.* **2014**, *35*, 417.
[44] R. J. Hickey, J. Koski, X. Meng, R. A. Riggleman, P. Zhang, S.-J. Park, *ACS Nano* **2014**, *8*, 495.
[45] Y. Geng, D. E. Discher, *J. Am. Chem. Soc.* **2005**, *127*, 12780.
[46] A. N. Lukyanov, T. A. Elbayoumi, A. R. Chakilam, V. P. Torchilin, *J. Controlled Release* **2004**, *100*, 135.
[47] Y. Zhong, C. Wang, L. Cheng, F. Meng, Z. Zhong, Z. Liu, *Biomacromolecules* **2013**, *14*, 2411.
[48] B. Surnar, M. Jayakannan, *Biomacromolecules* **2013**, *14*, 4377.
[49] P. P. Ghoroghchian, G. Li, D. H. Levine, K. P. Davis, F. S. Bates, D. A. Hammer, M. J. Therien, *Macromolecules* **2006**, *39*, 1673.
[50] F. Shi, J. Ding, C. Xiao, X. Zhuang, C. He, L. Chen, X. Chen, *J. Mater. Chem.* **2012**, *22*, 14168.
[51] P. L. Soo, L. Luo, D. Maysinger, A. Eisenberg, *Langmuir* **2002**, *18*, 9996.
[52] S. Papadimitriou, D. Bikiaris, *J. Controlled Release* **2009**, *138*, 177.